2017 IEEE International Conference on Robotics and Automation (ICRA)
DOI: 10.1109/ICRA.2017.7989185

Hitting the sweet spot: automatic optimization of energy transfer during tool-held hits

Jörn Vogel[1], Naohiro Takemura[2], Hannes Höppner[1], Patrick van der Smagt[3], Gowrishankar Ganesh[2,4]

***Abstract*— Tool-held hitting tasks, like hammering a nail or striking a ball with a bat, require humans, and robots, to purposely collide and transfer momentum from their limbs to the environment. Due to the vibrational dynamics, every tool has a location where a hit is most *efficient* results in minimal tool vibrations, and consequently maximum energy transfer to the environment. In sports, this location is often referred to as the "sweet spot" of a bat, or racquet. Our recent neuroscience study suggests that humans optimize hits by using the jerk and torque felt at their hand. Motivated by this result, in this work we first analyze the vibrational dynamics of an end-effector-held bat to understand the signature projected by a sweet spot on the jerk and torque sensed at the end-effector. We then use this analysis to develop a controller for a robotic "baseball hitter". The controller enables the robot-hitter to iteratively adjust its swing trajectory to ensure that the contact with the ball occurs at the sweet spot of the bat. We tested the controller on the DLR LWR III manipulator with three different bats. Like a human, our robot hitter is able to optimize the energy transfer, specifically maximize the ball velocity, during hits, by using its end effector position and torque sensors, and without any prior knowledge of the shape, size or material of the held bat.**

I. Introduction: A robot controller inspired by humans

Most popular tasks investigated in robotics and human motor neuroscience [1] are smooth, where the goal is either to purposefully avoid impacts or collisions [2], [3], [4], [5], [6], [7] with the environment, or to attenuate energy transfers, either from or to the environment, during unavoidable collisions and interactions [8], [9], [10]. In contrast, the goal of hitting tasks is to make purposeful collisions and maximize the energy transfer to the environment. Arguably, the end-effector impedance and tool movement trajectory play a crucial role in energy transfer during hits. However, the trajectory and impedance control, as well as energy optimization during hitting have been rarely investigated both, for humans in motor neuroscience, as well as in robotics.

Humans regularly perform hits with hand-held tools in the industry and in sports. The energy transfer in these tasks are known to be critically determined by the vibrational dynamics of the tool. In sports like baseball, cricket and tennis for example, players recognize that there is a location on the bat (or a racquet) where the impact with a ball sounds "sweet". Striking a ball in this location leads to least vibration at the hand, and maximizes the speed imparted to the ball.

[1]DLR Institute of Robotics and Mechatronics, Wessling, Germany, [2]Center for Information and Neural Networks (CINET), Osaka, Japan, [3]Volkswagen Group, Munich, Germany, [4]CNRS-AIST Joint Robotics Lab (UMI3218/RL), Tsukuba, Japan

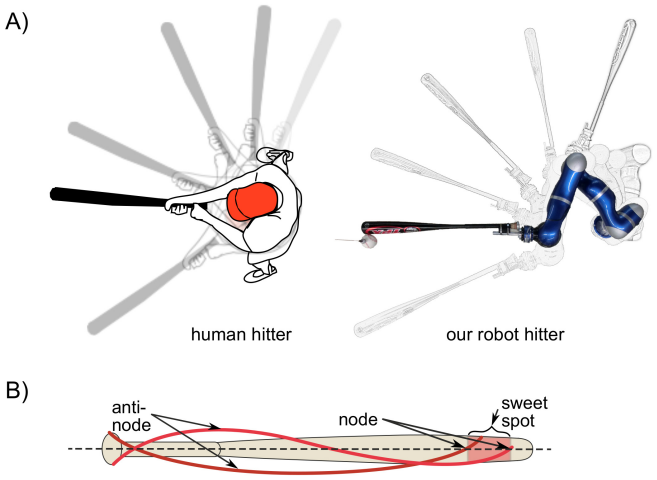

Fig. 1. **A) A top view of a human swinging the baseball bat and the swing produced by the LWR robot in our experiment. B) The *sweet spot* is a well known feature on a baseball bat where a ball impact leads to maximum transfer of momentum to the ball. Impacts lead to the excitation of multiple vibrational standing waves, or modes, in a bat. In a regular baseball bat, the sweet spot is near the "nodes" of the first two vibrational modes. where the two modes are excite the least.**

In colloquial terms, this location is called the *sweet spot* of the bat. Mechanically, the sweet spot exists because any impact excites multiple natural frequencies of mechanical vibrations in a bat. Each vibration is characterized by a natural mode (shape of vibration) with *anti-nodes*, where the vibration amplitudes are maximum, and *nodes* where the amplitudes are minimal (Fig. 1B). The extent to which any natural frequency is excited depends on the proximity of a hit to the antinode (of the natural mode) of a bat. The further from the antinode (and closer to the node) a ball hits, the lesser it excites the corresponding natural mode. The sweet spot usually lies towards the tip of the bat (Fig. 1B), near the nodes of natural modes (usually either the first and second, or second and third natural modes) where a hit would induce minimal vibrations of these natural frequencies. Striking a ball at the sweet spot thus ensures that the reflected energy lost in vibrating the bat is minimized, and consequently most of the input energy is transferred to the ball.

Human hitters (Fig. 1A), even novices, can immediately recognize when a ball does not hit the sweet spot, and importantly, intuitively recognize how to change their bat swing trajectory (and to a lesser extent, their hand impedance) in order to make the ball hit the sweet spot, and optimize

(maximize) the energy transfer to the ball. Arguably, they use the movement and force/torque feedback from their hands to achieve this, but until recently it was unclear what this feedback consists of, and how it is used to control and optimize hits.

In our recent motor neuroscience study we investigated how humans control and adapt hits with their limbs [11]. Our results suggest that humans are able to optimize energy transfer to an environment of unknown dynamics by minimizing (across hits) a weighted sum of the absolute force/torque and jerk perceived during impacts with the environment. In this study we extend this theoretical result to develop an automatic algorithm to enable a robot *hitter* (Fig. 1A) to optimize the energy transfer during tool-held hits, specifically when hitting a ball with end-effector-held bats.

Energy optimization of tool-held hits can be of utmost importance for robots because energy optimization not only maximizes the energy transfer to the environment, but probably more importantly, also minimizes energy reflection (in the form of vibrations and heat) to the robot. We hypothesize that the results from the neuroscience study, which were for direct limb impacts, are valid also when the hit is performed with a tool, and aimed to check whether and what signature of the sweet spot is observed in the torque and jerk at the end-effector. For this, we first analyzed and simulated the vibrational dynamics of a bat during a hit. We then examine how the impact torque and jerk sensed at the end-effector relate to the sweet spot on a bat. Finally we use this analysis to develop an iterative controller for a robotic hitter. We tested the controller on a DLR Light-Weight Robot (LWR) that hits an (initially stationary) ball with one of three bats (rods). The robot was unaware of the shape, size and dynamics of the bats and had no vision. Our controller enables the robot hitter to automatically adjust its swing trajectory across trials, and maximize the kinetic energy transferred to the ball like a human, using only the torque and jerk sensed at its end effector.

II. Bat Impact Physics

To develop the controller, we first analyzed the dynamics of a bat when it hits a ball. We assume the bat of length l is held at a revolute end-effector joint on the robot that can vary its rotational stiffness γ (Fig. 2).

We use the elementary beam theory, also called the Euler-Bernoulli beam theory, to derive the vibrational behavior of the bat [12]. This theory assumes that the angular distortion of the bat due to shear is small compared to the bending deformation, and thus, stipulates that the rotatory inertia can be ignored while analyzing bending. The theory is known to provide good approximations for beams with length to width ratios close to 20 or more, which arguably is the case with most bats.

Considering a small section of the bat (Fig. 2), and balancing the forces in the z direction,

$$-(V+dV)+f(x,t)dx+V=\rho A(x)\frac{\partial^2 w(x,t)}{\partial t^2} \qquad (1)$$

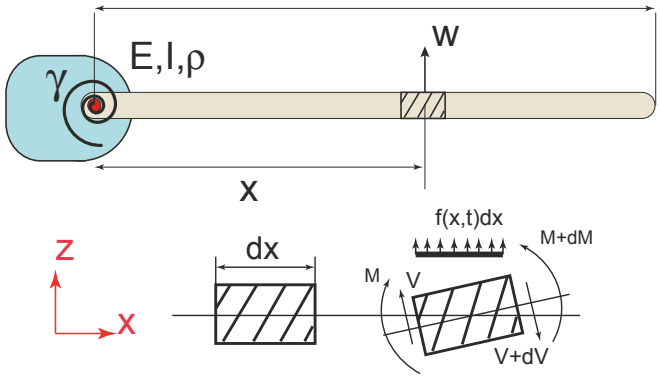

Fig. 2. **We analyzed a bat of length *l*, Young's modulus *E*, area moment of interia *I* and density ρ. The bat is assumed to be fixed to a rotational end-effector of stiffness γ Nm/rad. The forces and moments acting on an elemental section *dx* when the bat bends are shown below the bat. *f(x,t)* represents the external force, *V* represents the shear force, and *w* represents the lateral deflection of *dx*.**

where w represents the deflection about z, $V(x,t)$ is the shear force, $f(x,t)$ is the external force per unit length of the bat, ρ is the mass density and $A(x)$ is the cross sectional area of the beam at x. The moment about y leads to

$$(M+dM)-(V+dV)\,dx+f(x,t)\,dx\left(\frac{dx}{2}\right)-M=0 \qquad (2)$$

By writing $dV=\frac{\partial V}{\partial x}dx$ and $dM=\frac{\partial M}{\partial x}dx$ and disregarding terms involving second powers of dx in Eqs. (1) and (2) we get

$$-\frac{\partial V(x,t)}{\partial x}+f(x,t)=\rho A(x)\frac{\partial^2 w(x,t)}{\partial t^2} \qquad (3)$$

$$\frac{\partial M(x,t)}{\partial x}-V(x,t)=0 \qquad (4)$$

Substituting Eq. (4) in Eq. (3),

$$-\frac{\partial^2 M(x,t)}{\partial x^2}+f(x,t)=\rho A(x)\frac{\partial^2 w(x,t)}{\partial t^2} \qquad (5)$$

From the elementary theory of bending it is known that $M(x,t)=EI(x)\frac{\partial^2 w(x,t)}{\partial x^2}$, where E is the Young's modulus of the bat material and $I(x)$ is the area moment of inertia about the y axis at location x along the bat's length.

Substituting in Eq. (5),

$$\frac{\partial^2}{\partial x^2}\left[EI(x)\frac{\partial^2 w(x,t)}{\partial x^2}\right]+\rho A(x)\frac{\partial^2 w(x,t)}{\partial t^2}=f(x,t) \qquad (6)$$

We will first consider a bat of uniform cross-section and later show, by experiment, that our derivation also holds for non-uniform bats. For a uniform bat, Eq. (6) reduces to,

$$EI\frac{\partial^4 w(x,t)}{\partial x^4}+\rho A\frac{\partial^2 w(x,t)}{\partial t^2}=f(x,t) \qquad (7)$$

We model the bat ball impact with a double Dirac-Delta function of the form

$$f(x,t)=J\delta(x-p)\delta(t) \qquad (8)$$

where $x = p$ represents the location on the bat where the ball makes contact, and J is the scaling factor.

A. Homogeneous solution

Before solving this inhomogeneous equation (Eq. (7)), we will first solve the corresponding homogenous equation by setting $f(x,t)$ to zero,

$$EI\frac{\partial^4 w(x,t)}{\partial x^4} + \rho A\frac{\partial^2 w(x,t)}{\partial t^2} = 0 \tag{9}$$

The solution of Eq. (9) is of the form

$$\mathbf{w}_n'(x,t) = U_n \sigma_n(x)\sin(\omega_n t + \phi_n) \tag{10}$$

where $\sigma_n(x)$ and ω_n represent the *shape function* of the amplitude profile and the frequency of the n^{th} fundamental mode, respectively. U_n and ϕ_n represent the amplitude and phase characteristics of the vibration. The shape of a vibrating beam is known to be well approximated by a trigonometric function of the form

$$\begin{aligned}\sigma_n(x) =& a_n\sin(\beta_n x) + b_n\sinh(\beta_n x) \\ &+ c_n\cos(\beta_n x) + d_n\cosh(\beta_n x)\end{aligned} \tag{11}$$

where

$$\omega_n = {\beta_n}^2\sqrt{\frac{EI}{\rho A}} \tag{12}$$

The derivation of the shape of the n^{th} mode thus requires the evaluation of four constants, a_n, b_n, c_n, and d_n. We evaluated the constants using four boundary conditions, two at the revolute joint end, and two at the free end of the bat (Fig. 2).

At the revolute joint end ($x = 0$), we have zero deflection. Hence $w(0,t) = 0$. Substituting in Eq. (11) we get

$$0 = c_n + d_n \tag{13}$$

At the revolute joint end, the bending moment is balanced by the spring moment such that

$$EI\frac{\partial^2 w}{\partial x^2}\bigg|_{x=0} = -\gamma\frac{\partial w}{\partial x}\bigg|_{x=0} \tag{14}$$

with γ as the rotational stiffness; substituting in the differentials of Eq. (11),

$$EI\beta_n(-c_n + d_n) = -\gamma(a_n + b_n) \tag{15}$$

At the free end ($x = l$), the bending moment is zero:

$$\frac{\partial^2 w}{\partial x^2}\bigg|_{x=l} = 0 \tag{16}$$

substituting in the differentials of Eq. (11), we get

$$-a_n\sin(\beta_n l) + b_n\sinh(\beta_n l) - c_n\cos(\beta_n l) + d_n\cosh(\beta_n l) = 0 \tag{17}$$

Finally, the shear force $\frac{\partial}{\partial x}\left(EI\frac{\partial^2 w}{\partial x^2}\right)\Big|_{x=l} = 0$ at the free end, this means

$$-a_n\cos(\beta_n l) + b_n\cosh(\beta_n l) + c_n\sin(\beta_n l) + d_n\sinh(\beta_n l) = 0 \tag{18}$$

Collecting Eqs. (13), (15), (17), and (18), and rearranging we get

$$\mathbf{Q}\begin{bmatrix} a_n & b_n & c_n & d_n\end{bmatrix}' = 0 \tag{19}$$

where

$$\mathbf{Q} = \begin{bmatrix} 0 & 0 & 1 & 1 \\ \frac{\gamma}{EI\beta_n} & \frac{\gamma}{EI\beta_n} & -1 & 1 \\ -\sin(\beta_n l) & \sinh(\beta_n l) & -\cos(\beta_n l) & \cosh(\beta_n l) \\ -\cos(\beta_n l) & \cosh(\beta_n l) & \sin(\beta_n l) & \sinh(\beta_n l)\end{bmatrix} \tag{20}$$

and, as equation Eq. (19) definitively has non-trivial solutions, we know that

$$\det|\mathbf{Q}| = 0 \tag{21}$$

Equation (21) can be used to numerically evaluate possible values of β_n, and hence ω_n (12), each corresponding to a natural frequency. Eqs. (19) and (20) can then be used to solve for the shape function (Eq. (11)), and thus to evaluate the homogeneous dynamics of each natural mode (Eq. (10)).

B. Inhomogeneous solution

Next, we solve for the particular solution, or inhomogeneous solution, of Eq. (8). For this we consider a candidate function that is the product of the shape function $\sigma_n(x)$ and an arbitrary function in time $\psi_n(t)$ given by

$$\theta_n(x,t) = \sigma_n(x)\psi_n(t) \tag{22}$$

Substituting in Eq. (7) from Eq. (8) and Eq. (22), we get

$$EI\beta_n^4\sigma_n(x)\psi_n(t) + \rho A\sigma_n(x)\ddot{\psi}_n(t) = J\delta(x-p)\delta(t) \tag{23}$$

multiplying both sides by $\sigma_n(x)$ and integrating, we get

$$\begin{aligned}\left[EI\beta_n^4\psi_n(t) + \rho A\ddot{\psi}_n(t)\right]\int_0^L \sigma_n(x)^2 dx = \\ J\int_0^L \delta(x-p)\delta(t)\sigma_n(x)dx\end{aligned} \tag{24}$$

or

$$EI\beta_n^4 H_n^\sigma\psi_n(t) + \rho A H_n^\sigma\ddot{\psi}_n(t) = J\sigma_n(p)\delta(t) \tag{25}$$

where, $H_n^\sigma = \int_0^L \sigma_n(x)^2 dx$. Eq. (25) is a second-order differential equation in $\psi_n(t)$ which has the solution

$$\psi_n(t) = \frac{J\sigma_n(p)}{\rho A H_n^\sigma\omega_n}\sin(\omega_n t) \tag{26}$$

where ω_n is as in Eq. (12). The particular solution thus becomes

$$\theta_n(x,t) = \frac{J\sigma_n(p)}{\rho A H_n^\sigma\omega_n}\sigma_n(x)\sin(\omega_n t) \tag{27}$$

With this we have the complete dynamics of the bat at impact, which is given by the summation of Eq. (10) and Eq. (27)

$$\begin{aligned}\mathbf{w}_n(x,t) = \sum_{n=1}^{\infty}\Bigg[&U_n\sigma_n(x)\sin(\omega_n t + \phi_n) \\ &+ \frac{J\sigma_n(p)}{\rho A H_n^\sigma\omega_n}\sigma_n(x)\sin(\omega_n t)\Bigg]\end{aligned} \tag{28}$$

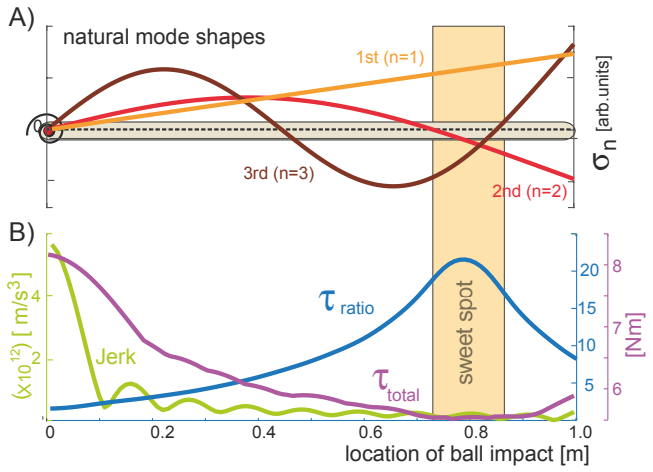

Fig. 3. **A) A ball impact on the bat induces multiple natural modes of vibration. The figure shows the mode shapes (σ_n) of the first three natural modes when the ball hits at $p = 0.78$ m from the end-effector. B) A plot of the change in τ_{total} (purple), τ_{ratio} (blue) and Jerk (green) with the location of ball impact shows that the total torque is minimal, and the torque ratio is maximum around $p = 0.78$ m from the end-effector where the second and third modes have minimal amplitudes.**

Note that the amplitude U_n and phase ϕ_n are external parameters that are determined by the initial deflection of the bat. As our robot hitter has limited joint acceleration, we can assume the bat deflection before impact to be negligible and hence set both U_n and ϕ_n to zero.

III. The Sweet Spot Signature

Our purpose of the above bat impact dynamics analysis is to understand and extract the appropriate position and/or force/torque signature at the end-effector, that can inform our robot (controller) where a ball has hit the bat with respect to the sweet spot. For this, we started by numerically simulating the shape function of a bat of length $l = 1$ m, Young's modulus $E = 13\,\text{GN/m}^2$ (corresponding to wood), density $\rho = 700\,\text{kg/m}^3$, a circular cross section of diameter 6.0 cm, and a relatively high robot end-effector stiffness of $\gamma = 500$ Nm/rad. We considered the first ten natural frequencies of vibration in the bat but found that 99.9% of the vibrational energy was contained in the first three natural frequencies of 4 Hz, 225 Hz, and 727 Hz, respectively. Using Eq. (11), the first three natural modes were obtained as shown in Fig. 3A.

Next we analyzed how the position and torque feedback at the end-effector (hand) changes when the ball impacts the bat at different locations along its length. For this we simulated the bat dynamics (Eq. (28)) for $p = [0, 1]$, assuming a constant peak impact reaction torque ($pXJ = 10$ Nm) at the end-effector. Our human studies [11] suggested the jerk and reaction torque induced by the impact to be possible sensory components that show some systematic change depending on where the ball hits the bat. Angular jerk amplitude can be estimated at the end-effector $x = 0$ through

$$\text{Jerk} = \left\| \frac{\partial \ddot{\mathbf{w}}_n(0,t)}{\partial x} \right\| \tag{29}$$

where $\|.\|$ represents the square of the amplitude. The torque amplitude induced by the vibrations at the end effector was calculated as

$$\tau_{\text{total}} = \gamma \left\| \frac{\partial \mathbf{w}(0,t)}{\partial x} \right\| \tag{30}$$

Finally, we also analyze the torque ratio (τ_{ratio}) between the torque amplitude induced by the first mode and the torque amplitudes induced by the rest of the modes. With $F_c[.]$ representing the low-pass filter function with cut-off frequency c such that $\omega_1 < c < \omega_2$, we calculated the torque ratio as

$$\tau_{\text{ratio}} = \frac{\gamma \| \partial F_c\left[\mathbf{w}(0,t)\right]/\partial x \|}{\gamma \| \partial (\mathbf{w}(0,t) - F_c\left[\mathbf{w}(0,t)\right])/\partial x \|} \tag{31}$$

The Jerk, τ_{total} and τ_{ratio} calculated for different ball impact locations are plotted in Fig. 3B.

The τ_{total} was observed to be minimum when the ball impact was at $p = 0.78$ m, which corresponds to where the second and third modes have minimum shape amplitude σ (Fig. 3A). Minimum τ_{total} indicates that the vibrations of the bat were minimal when the ball hit this location, and represents the sweet spot of this bat. However, we observed that the change in total torque is relatively small (< 3 Nm; see purple trace in Fig. 3B) with change in ball impact location, making it susceptible to noise during real experiments.

In comparison, τ_{ratio} was observed to exhibit a more prominent change over the ball impact locations (see blue trace in Fig. 3B), and crucially, observed to peak at the sweet spot. The reason why the peak τ_{ratio} and that minimum τ_{total} occur at the same impact location is not intuitive. This happens due to the fact that most of the vibrational energy in an impact is taken by the first mode of vibration, which shows a monotonically changing amplitude for most bats (see orange trace in Fig. 3A). In fact, the simulations reveal that τ_{ratio} can track the sweet spot for different bats irrespective of the impact force, and irrespective of the length, cross-section and material properties of the bat (See Fig. 4). This, in addition to the critical fact that τ_{ratio} provides (at least in theory) a smooth convex function (Fig. 3B and Fig. 4) in terms of ball impact location, makes it an appropriate variable to locate the sweet spot on the bat (see Sec. IV-C).

On the other hand, Jerk exhibits a decreasing function in ball impact location for bats of uniform cross section (see green trace in Fig. 3B). However, we still chose to use Jerk in our iterative controller (Sec. IV-C) because in preliminary experiments we noticed that minimum Jerk tracks the sweet spot in the case of non-uniform bats, such as the baseball bat (see green trace in Fig. 6).

IV. Robot Experiments

We implemented our *robot hitter* on a DLR Light-Weight-Robot III robotic platform. The robot worked with one of three bats of different shape, size and material (Fig. 5):

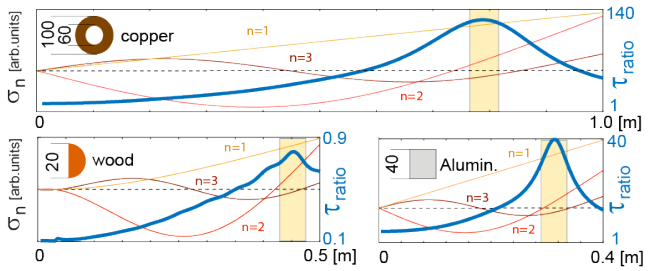

Fig. 4. **The modes and τ_{ratio} plotted similar to Fig. 3 for a cylindrical hollow copper bat of 1 m length, a semi-circular cross-section wooden bat of 0.5 m length, and a square cross-section aluminum bat of 0.4 m length. The τ_{ratio} peaks at the sweet-spot (marked in orange), determined as the location where τ_{total} (not shown in the plot) is minimum, on all the bats.**

- a wooden rod (A=2 cm × 3 cm; L=0.9 m; with the 3 cm face hitting the ball);
- a copper rod (D=2 cm; d=1.6 cm; L=0.75 m);
- a regular baseball bat.

A 6-DoF force–torque sensor at the mounting of the bat allowed us to measure the vibrational forces and torques at the end-effector of the robot. The ball to be hit was hung from the ceiling by a string of length 2.75 m (See Fig. 5 and video attachment). A passive reflective Vicon marker attached to the ball allowed for it to be tracked during the hits.

A. Swing trajectory

The robot was programmed to execute bat swings to hit the ball. The ball impact location on the bat was modified by changing the robot configuration; specifically the rotation of joints q_1, q_4 and q_6 (see Fig. 5). We will denote a chosen configuration (which corresponds to a particular ball impact location) by the value θ_{hit}. The joint limits of the robot allowed us to shift the position of the bat, and thereby have the ball hit the bat at different locations, over a range of 0.3 m along its longitudinal axis.

The bat swing was executed by joints q_1 and q_6. The swing started at θ_{start} (see Fig. 5) and the ball contact occurred at θ_{hit} (see Fig. 5). The swing trajectory was defined such that the joint configuration θ_{hit} was centered between θ_{start} and θ_{end}. A same range of motion and speed of the joints q_1 and q_6 were chosen in each swing ($\Delta q_1 = \Delta q_6; \dot{q}_1 = \dot{q}_6$) to ensure that the bat and ball contact occurs when the task space bat velocity is perpendicular to the axis of the bat.

The robot joints were driven to a constant pre-calculated joint velocity (explained in Sec. IV-B) in each hit using a joint impedance controller [13]. Crucially, the impedance controller was turned off (and the robot transferred to zero gravity, zero friction control) as soon as the contact with the ball was detected. The swing controller runs at 1 kHz (in comparison the impact lasted < 50 ms) and the turnoff was performed using a threshold of 20000 Nm/s on the derivative of the torque signal induced during the ball hit. This switching was crucial to ensure that the impedance

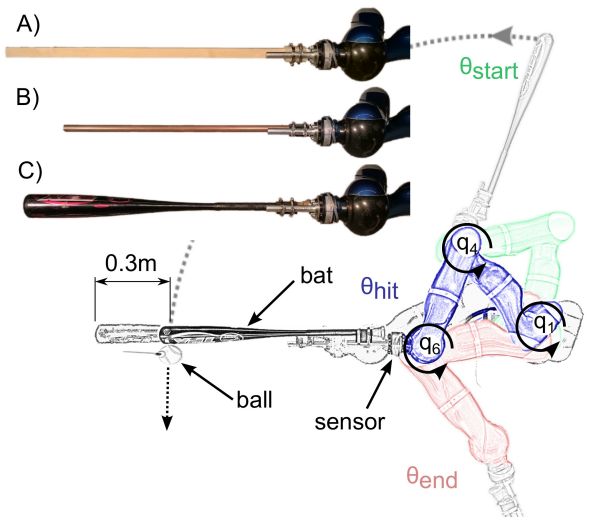

Fig. 5. **Robot setup and exemplary joint configurations. By moving joins q_1, q_4 and q_6 the robot hitter can cover a translatory range of 0.3 m. A) Wooden bat. B) Copper bat. C) Baseball bat.**

controller does not compensate for the energy loss during ball impact, and allowed us to control the input energy to the robot hitter and ball system by fixing the joint velocities at the point of impact.

B. Controlling input energy to the robot-hitter and ball system

In order to clearly exhibit the energy transfer maximization (to the ball) by our robot, we chose to provide a constant predefined energy input to the robot hitter in each hit. This was done by adjusting the robot joint velocities before impact according to the inertia of the robot system (configuration) chosen for that hit.

The inertia of the robot is lowest when it is least extended (when joint angles q_1 and q_6 are minimum, and q_4 is maximum). We chose a joint velocity of $\dot{q}_1 = \dot{q}_6 = \pi/2$ rad/s for this configuration. The velocities of the other joints were always zero.

The total kinetic Energy E_{kin} of the robot when hitting the ball can be evaluated as:

$$E_{\text{kin}}(\theta_{\text{hit}}, \dot{q}_1, \dot{q}_6) = E_{\text{kin\_link}} + E_{\text{kin\_motor}}\,, \tag{32}$$

where $E_{\text{kin\_link}}$ is the kinetic energy of the robots links and $E_{\text{kin\_motor}}$ is the kinetic energy stored in the rotating parts of the motor and are given by.

$$E_{\text{kin\_link}} = \frac{1}{2}[\,\mathbf{I}_{1,1}(\theta_{\text{hit}})\dot{q}_1^2 + (\mathbf{I}_{6,1}(\theta_{hit}) + \mathbf{I}_{1,6}(\theta_{\text{hit}}))\dot{q}_1\dot{q}_6 + \mathbf{I}_{6,6}(\theta_{\text{hit}})\dot{q}_6^2\,] \tag{33}$$

$$E_{\text{kin\_motor}} = \frac{1}{2}[\,\mathbf{I}_{M1}(\dot{q}_1 r_1)^2 + \mathbf{I}_{M6}(\dot{q}_6 r_6)^2\,] \tag{34}$$

Here, $\mathbf{I}_{i,j}(\theta_{hit})$ is the i-th row j-th column entry of the inertia matrix $\mathbf{I}$ of the robot hitter (the robot and bat) in

configuration (θ_{hit}), $\mathbf{I}_{Mi}$ is the i-th motor inertia and r_i is the respective gear ratio.

The total kinetic energy of our robot hitter in this configuration was calculated as E_{const} Joules for each bat. To ensure the input of the same energy for every hit, the desired $\dot{q}_1$, $\dot{q}_6$ for any robot configuration θ_{new} was then calculated as

$$\dot{q}_1 = \dot{q}_6 = \sqrt{\frac{2E_{\text{const}}}{Z}} \tag{35}$$

$$\begin{aligned} Z = {} & \mathbf{I}_{1,1}(\theta_{\text{new}}) + \mathbf{I}_{6,1}(\theta_{\text{new}}) + \mathbf{I}_{1,6}(\theta_{\text{new}}) \\ & + \mathbf{I}_{6,6}(\theta_{\text{new}}) + \mathbf{I}_{M1} r_1^2 + \mathbf{I}_{M6} r_6^2 \end{aligned} \tag{36}$$

C. A cost function of Jerk and T_{ratio}

Based on our analysis of the sensory signature of the sweet spot (Sec. III), and the observation in preliminary experiments that minimum angular jerk can track the sweet spot in non-uniform bats, we developed a cost function including T_{ratio} and angular jerk for our iterative controller to minimize. Angular jerk was calculated at the sixth joint (q_6) of the robot using Eq. (29), while T_{ratio} was calculated using Eq. (31) on the the readings of torque by the force-torque sensor on the robot end-effector. As jerk is minimum, and T_{ratio} is maximum at the sweet spot, the cost function was developed by subtracting T_{ratio} from Jerk

$$H_{\text{cost}} = \alpha \, \text{Jerk}(q_6) - T_{\text{ratio}}(\tau_{\text{sensor}}, c). \tag{37}$$

Where $\alpha = 50.000$ is a weight parameter to adjust for the different scaling of the two cost components. c represents the cut-off frequency (see Eq. (31)) and was taken as 125 Hz for all the bats.

First, we evaluated the validity of this theoretically derived cost function for our real hitting task by systematically testing the value of the cost function for ball impacts (made by the robot) every 2 cm from the tip of a bat. The ball impacts were achieved by changing the swing trajectory as explained in Sec. IV-A by equalizing the input energy to the robot-hitter (Sec. IV-B).

Figure 6-A shows the velocity of the impact point on the bat (brown trace), ball velocity (orange trace) and the value of the cost function (Eq. (37)) calculated along the length of the wooden bat. The ball velocity was observed to be maximum when the impact was 0.70 m from the handle. This is arguably the sweet spot of this bat. Interestingly, note that the bat velocity on impact at this spot is in fact smaller than on impact at the tip of the bat exhibiting that the ball velocity is not determined simply by the bat velocity at impact. Critically for us, we observed that the cost function is indeed minimum when the impact is at the sweet spot.

Figures 6-B and C depict the bat (contact point) velocity, ball velocity and the value of the cost function when using a copper tube or a regular baseball bat, respectively. Similar behavior as with the wooden bat can be observed. However, it is evident that the baseball bat is designed to have the sweet spot closer to the tip. The value of the Jerk component of the cost function is plotted for the baseball bat (green trace) to show that minimum Jerk can locate the sweet spot of non-uniform bats.

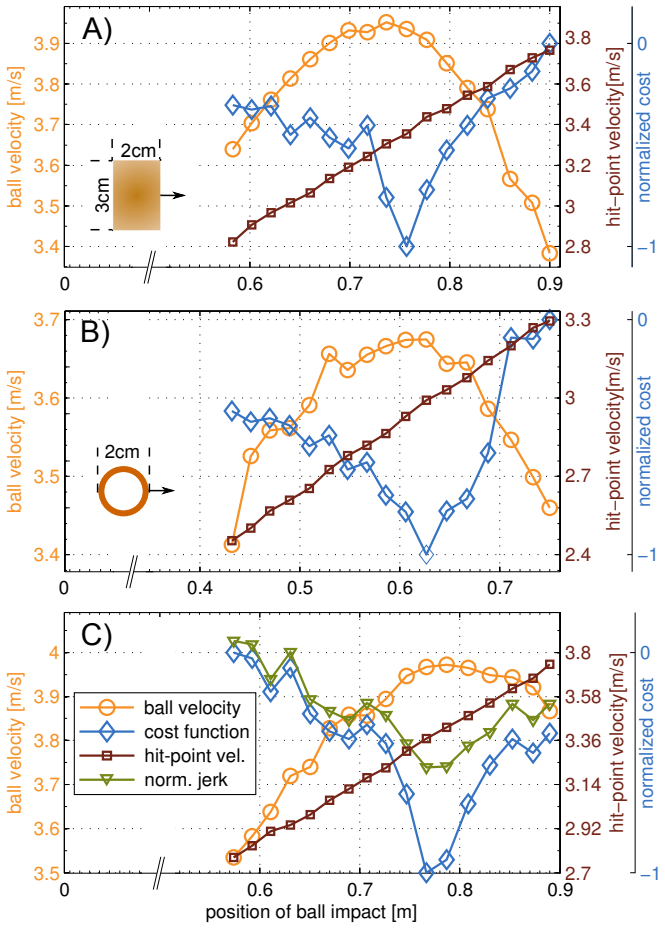

Fig. 6. **Hitting a A) tennis ball with the square wooden rod as a bat, B)a tennis ball with a copper tube, and C)a baseball with a baseball bat. Position 0 refers to the handle of the bat. Brown squares indicate the velocity of the impact location of the bat (at impact), orange circles depict the velocity of the ball right after the impact, blue diamonds depict the value of the cost function. We append the normalized Jerk component of the cost function recorded for the baseball bat to show that minimum Jerk can track the sweet spot in the case of non-uniform bats.**

D. Automatic localization for hitting the sweet spot

Following the verification of the cost function, we developed an iterative controller using this cost function to enable our robot hitter to automatically modify the swing trajectory to hit the sweet spot, and thereby maximize the ball velocity. The controller estimates the cost function recursively after each hit using a cubic polynomial of the form

$$H_{\text{cost}}(x) = \zeta_1 x^3 + \zeta_2 x^2 + \zeta_3 x + \zeta_4, \quad x = [0, 0.3] \tag{38}$$

where the coordinate x is constrained by the translatory range (of 0.3 m) available to the robot. Our robot starts by first choosing three initial impact positions: two at the limits of the translatory range and one at one-third of the distance between these limits (see Fig. 5). Following the first three impacts, before every subsequent swing, the cost calculated in all the preceding impacts is used to compute a least square estimate of the parameters $\zeta_1, \zeta_2, \zeta_3$ and ζ_4, and hence the

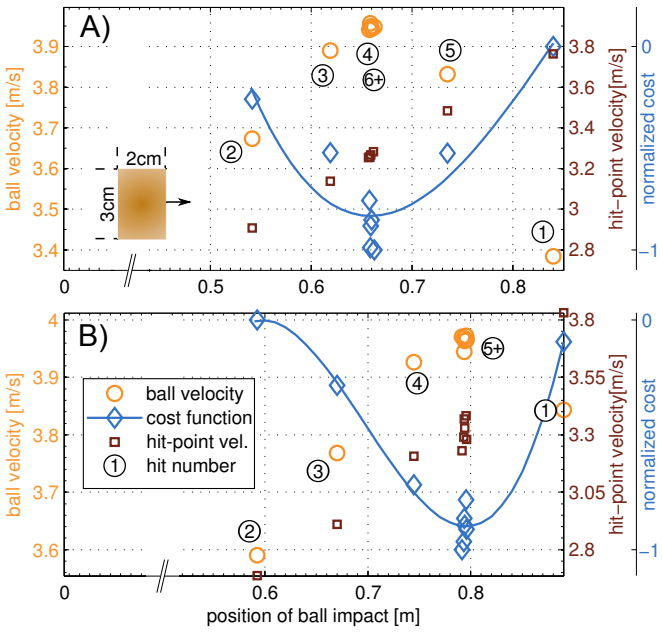

Fig. 7. **A) Hitting a tennis ball with the square wooden bat, and B)baseball bat using the iterative controller to converge to the sweet spot of the bat over nine swings. The bat (contact point) velocity, ball velocity and cost function are indicated in brown, orange and blue as before. The integers indicate the swing number and the solid curve represents the estimated cost function after the ninth swing.**

cost function polynomial (see 38), using a Moore-Penrose *pseudo-inverse*. It has to be noted that the initial three data points leave the cubic polynomial underconstrained at first. However, given the properties of a cubic polynomial and the characteristics of our cost function, it is evident that the local minimum of this initial fit is located within the range of motion of the robot and can therefore be used as a starting point for the iterative optimization. We selected this polynomial minimization procedure because of its computational simplicity and speed of convergence and importantly because we found it to be sufficiently robust to the noise in the cost function across different bats.

Figure 7-A shows hit points for 9 swings with the wooden bat, made to hit a tennis ball. The integers on the figure indicate the swing number. The bat (contact point) velocity, ball velocity and cost function are indicated for each swing. The cost function estimation generated by the controller after the ninth swing is shown by the solid blue trace. It is evident, that our robot hitter converged to the optimal hit-point by the 6th hit. Figure 7-B shows the convergence when the robot uses a regular baseball bat to hit a baseball. The robot-hitter is able to converge to the sweet spot within 5 swings in this case.

We note here that while our chosen convergence procedure (and particularly the choice of a polynomial of third degree) works well for our setup, other robust gradient descent or binary search procedures may be more suitable for robots with longer translatory ranges. However, while different algorithms can be used for the convergence, the critical contribution of this work is in regard to the cost function (Eq. (37)) which enables the iterative controller to maximize the energy transfer (ball velocity in our case) without requiring information about the size, shape and the dynamic properties of the bat it is hitting with and without tracking the manipulated environment.

V. Discussion

Humans are adept at most motor tasks and previous studies have shown how understanding and implementing human inspired control can benefit robots [14], [15], [16]. Here we developed an iterative controller that enables a robot hitter to optimize energy transfer during a tool-held hit, similar to a human. The human experiments on this issue were performed on limb hits (without tools) and suggested that the jerk and torque, perceived in some unspecified form at the hand, are useful to optimize hits. The key challenge for this study was to examine whether the same feedbacks are valid for energy optimization of tool-held hits (specifically for localizing the sweet spot on the tool), and if so to find a signature of the sweet spot in the jerk and torque observed at the end-effector.

We analyzed the vibrational dynamics of an end-effector-held bat and observed that the torque ratio, and to a lesser extent angular jerk, sensed at the end-effector, can be utilized to locate the sweet spot on a bat. However, our analysis was performed with several assumptions. The bat was assumed to be a "Euler Bernoulli" beam of uniform cross-section, the vibrations were assumed to be planar, and the vibrational damping effects were ignored in the jerk calculations. We verified the validity of these assumptions for real life tool hit tasks by developing an iterative controller for a robot hitter. Like a human, our robot hitter is able to optimize the energy transfer, specifically maximize ball velocity, without any prior knowledge of the shape, size or material of the held bat. Overall our experiments helped demonstrate that:

- The assumptions in our analysis are acceptable;
- Torque ratio and angular jerk are sufficiently robust indicators of the sweet spot during real life tool use;
- Torque ratio and angular jerk can be used to isolate the sweet spot on not just uniform cross-section, but also bats of non-uniform cross-section;
- Maximization of energy transfer is achieved without observation of the manipulated environment (ball in our case);
- The ball velocities observed in the experiments confirmed that a hit at the sweet spot optimizes energy transfer to the environment.

This paradigm, where a robot hits a ball with a bat, itself is of course not new and has been examined in previous studies [17], [18], [19] in robotics. But these studies have concentrated on maximizing hit velocity [17] or achieving a proper bat–ball contact [18], [19]. On the other hand, here we concentrated on the optimization of energy transfer through the adaptation of the swing trajectory (and hence the impact location) of the hits. A related issue that we analyzed but do not present here is that of end-effector stiffness, and its effect

on this optimization. End point stiffness changes can lead to changes in the sweet spot of a tool, and conversely, can be used actively to modify the sweet spot of a tool. The robot end point stiffness (in fact impedance) critically determines the velocity maximization of the robot swing, an issue that has been addressed in previous studies that investigated throwing [20] and hitting [17] by robots. Our next goal is to develop an integrated controller (combing results of these studies) for a variable impedance actuated robot hitter, that can localize a moving ball and both, maximize bat swing velocity as well as the energy transfer to the ball simultaneously. By doing this, the robot hitter's skill would come close to the human skill with bats in sports, and tools in general.

VI. Acknowledgement

NT, PvS and GG were supported by the AMED-DFG/BMBF Japanese-German Computational Neuroscience project. NT and GG were partially supported by NICT Japan. We would like to thank Martin Görner for proofreading previous versions of this document.

References

[1] D. Wolpert, J. Deidrichsen, and R. Flanagan, "Principles of sensorimotor learning," *Nature Neuroscience Reviews*, vol. 12, no. 12, pp. 739–751, 2011.

[2] A. D. Luca, A. Albu-Schaffer, S. Haddadin, and G. Hirzinger, "Collision detection and safe reaction with the dlr-iii lightweight manipulator arm," in *2006 IEEE/RSJ International Conference on Intelligent Robots and Systems*, Oct 2006, pp. 1623–1630.

[3] F. Flacco, T. Kröger, A. D. Luca, and O. Khatib, "A depth space approach to human-robot collision avoidance," in *Robotics and Automation (ICRA), 2012 IEEE International Conference on*, May 2012, pp. 338–345.

[4] M. Zago, J. McIntyre, P. Senot, and F. Lacquaniti, "Visuomotor coordination and internal models for object interception," *Experimental Brain Research*, vol. 192, no. 4, pp. 571–604, 2009. [Online]. Available: http://dx.doi.org/10.1007/s00221-008-1691-3

[5] J. Vaughan, D. A. Rosenbaum, and R. G. J. Meulenbroek, "Planning reaching and grasping movements: The problem of obstacle avoidance," *Motor Control*, pp. 116–135, 2001.

[6] A. F. d. C. Hamilton and D. M. Wolpert, "Controlling the statistics of action: Obstacle avoidance," *Journal of Neurophysiology*, vol. 87, no. 5, pp. 2434–2440, 2002. [Online]. Available: http://jn.physiology.org/content/87/5/2434

[7] M. Mon-Williams, R. J. Tresilian, L. V. Coppard, and G. R. Carson, "The effect of obstacle position on reach-to-grasp movements," *Experimental Brain Research*, vol. 137, no. 3, pp. 497–501, 2001. [Online]. Available: http://dx.doi.org/10.1007/s002210100684

[8] G. De Magistris, A. Pajon, S. Miossec, and A. Kheddar, "Humanoid walking with compliant soles using a deformation estimator," in *International Conference on Robotics and Automation (ICRA)*, 2016.

[9] H. Kaminaga, J. Englsberger, and C. Ott, "Kinematic optimization and online adaptation of swing foot trajectory for biped locomotion," in *2012 12th IEEE-RAS International Conference on Humanoid Robots (Humanoids 2012)*. IEEE, 2012, pp. 593–599.

[10] S. Haddadin, A. Albu-Schaffer, A. D. Luca, and G. Hirzinger, "Collision detection and reaction: A contribution to safe physical human-robot interaction," in *2008 IEEE/RSJ International Conference on Intelligent Robots and Systems*, Sept 2008, pp. 3356–3363.

[11] N. Takemura, P. Korhammer D, van der Smagt, and G. Ganesh, "Towards measurement and understanding of human impedance control during voluntary impacts," in *Presentation at the Neural control of Movement (NCM)*. Society of Neural control of movement, 2015.

[12] L. Meirovitch, *Fundamentals of vibrations*. Waveland Press, 2010.

[13] A. Albu-Schäffer, C. Ott, and G. Hirzinger, "A unified passivity-based control framework for position, torque and impedance control of flexible joint robots," *The International Journal of Robotics Research*, vol. 26, no. 1, pp. 23–39, 2007.

[14] E. Burdet, G. Ganesh, and A. Albu-Schaffer, "Interaction Force , Impedance and Trajectory Adaptation : by Humans , for Robots," in *ISER 2010*, 2010.

[15] C. Yang, G. Ganesh, and S. Haddadin, "Human-like Adaptation of Force and Impedance in Stable and Unstable Interactions," *Transaction Robotics*, pp. 1–12, 2011.

[16] G. Ganesh, N. Jarasse, S. Haddadin, A. Albu-Schaffer, and E. Burdet, "A versatile biomimetic controller for contact tooling and haptic exploration," in *Robotics and Automation (ICRA), 2012 IEEE International Conference on*. IEEE, 2012, pp. 3329–3334. [Online]. Available: http://ieeexplore.ieee.org/document/6225057/?arnumber=6225057

[17] X.-Z. Zheng, W. Inamurat, K. Shibata, and K. Ito, "A Learning and Dynamic Pattern Generating Architecture for Skillful Robotic Baseball Batting System," in *Robotics and Automation (ICRA), 2000 IEEE International Conference on*. IEEE, 2000, pp. 3227–3232. [Online]. Available: http://ieeexplore.ieee.org/document/845160/?arnumber=845160

[18] T. Senoo, A. Namiki, and M. Ishikawa, "High-speed Batting Using a Multi-Jointed Manipulator," in *Robotics and Automation (ICRA), 2004 IEEE International Conference on*. IEEE, 2004, pp. 1191–1196. [Online]. Available: http://ieeexplore.ieee.org/document/1641961/

[19] J. Peters and S. Schaal, "Policy gradient methods for robotics," in *2006 IEEE/RSJ International Conference on Intelligent Robots and Systems*, Oct 2006, pp. 2219–2225.

[20] S. Haddadin, F. Huber, and A. Albu-Schäffer, "Optimal control for exploiting the natural dynamics of variable stiffness robots," in *Robotics and Automation (ICRA), 2012 IEEE International Conference on*. IEEE, 2012, pp. 3347–3354.